JOURNAL OF MATERIALS SCIENCE 22 (1987) 3581–3588

Advanced P/M aluminium alloy: rapidly quenched structure and decomposition behaviour during annealing

G. J. MARSHALL*
Department of Metallurgy and Material Science, Imperial College, London SW7 2BP, UK

An Al–Fe–Cr–Zr alloy is currently being developed for elevated temperature service utilizing rapid solidification technology. The inert gas atomized powder has been assessed microstructurally and the solidification behaviour interpreted as a function of particle size. It was significant that both fine and coarse powders exhibited structures created by solute trapping during the initial stages of solidification. An unidentified phase (or possibly phases) was detected by X-ray and electron diffraction and shown to form at cell boundaries. Zirconium was retained in solid solution during solidification of all powder structures and subsequently precipitated as fine particles of the metastable Al_3Zr phase during heat treatment. This precipitation was extremely fine and deemed suitable for elevated temperature strengthening. In contrast, the iron and chromium additions partition to the cell boundaries and precipitate during heating to their respective equilibrium compounds.

1. Introduction

Current aluminium alloy developments utilize rapid solidification techniques to produce materials suitable for elevated temperature service beyond present limits. The principle objective is the replacement of titanium components in airframe and aeroengine applications thus achieving considerable weight savings [1].

Rapid solidification allows the addition of transition elements to aluminium which have low solid state diffusivity and low equilibrium solid solubility and can, in a suitably processed component, create desirable properties by the formation of stable intermetallic dispersoids. Among the most successful development alloy systems are those based on Al–Fe–X [2] and Al–Cr–Zr [3]. P/M Al–Fe alloys owe their elevated temperature strength to fine, metastable Al–Fe particles formed during rapid solidification; however, structural inhomogeneities and the initial high hardness create processing difficulties [3]. In contrast, the Al–Cr–Zr alloys are reported [4] to be easier to fabricate and attain strength during or after processing from the precipitation of a coherent metastable Al_3–Zr phase. However, in comparison to the Al–Fe system, very little has been published regarding the Al–Cr–Zr alloys. Theoretical considerations suggested that an alloy combining the two systems but with reduced solute content should provide an easily consolidated material with good elevated temperature strength and adequate toughness.

The objective of this communication is the examination of the solidification structure of an Al–Fe–Cr–Zr powder produced by inert gas atomization. In addition, the decomposition behaviour has been assessed during annealing of the powder.

2. Experimental procedure

The powder was produced by inert gas atomization at Metalloys UK and had a melt composition of Al–2.59Fe–3.30Cr–1.30Zr (wt %). The particle size distribution and an example of the powder morphology are given in Fig. 1. (It should be noted that the batch of powder examined had been screened at 53 μm.)

To enable a thorough examination of the powder with particular regard to particle size, three size fractions were prepared from the original batch. The separation technique into +40, +12 to 25 and −6 μm fractions and the subsequent sample preparation for transmission electron microscopy (TEM) have been given previously [5]. The high voltage (1 MeV) electron microscope (HVEM) facility has been used extensively for microstructural characterization and where appropriate microanalysis was performed on a Jeol 120CX TEMSCAN using a Links systems analyser incorporating standard thin foil correction programmes.

Phase identification within powder fractions was carried out using a Philips X-ray Diffractometer employing Cu$K\alpha$ radiation at 40 keV and 30 mA.

Microstructural transformations during annealing of the powder were assessed by batch heating at 350, 450 and 550° C and by *in situ* heating at 400 and 450° C. The nickel foil technique was unsuitable for *in situ* heating in the HVEM and hence powder was pressed to near full density at 350° C and then electron-transparent samples prepared by electropolishing. The batch heating process indicated that 1 h at 350° C

* *Present address*: Alcan International, Banbury, Oxon OX16 7SP, UK.

0022–2461/87 $03.00 + .12

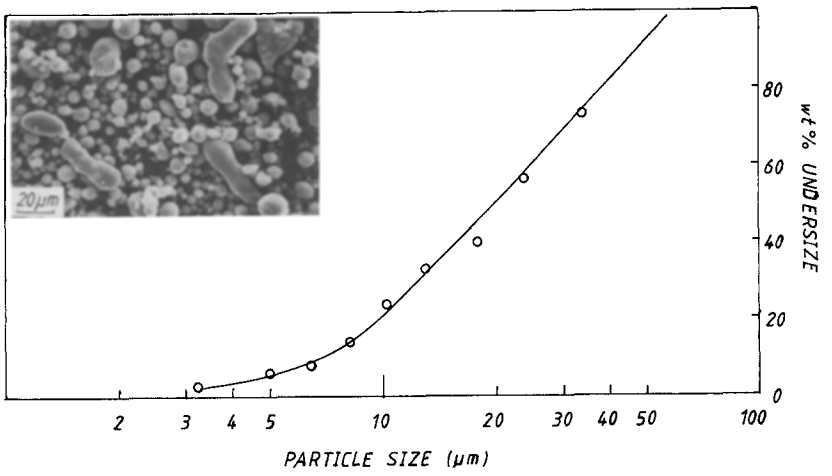

Figure 1 Powder size distribution and morphology.

did not alter the original microstructure and so the compaction process was suitable for reliable *in situ* heating experiments.

3. Results and discussion

3.1. Powder microstructure

Preliminary details of the as-received powder microstructures were presented at a recent conference [5]; however, the solidification behaviour was not discussed in great detail. Moreover, there are several microstructural features worth reviewing and examples will be given but the reader may wish to refer to the earlier publication [5].

In general, the powers exhibited either cellular or structurally featureless morphologies but most commonly a mixture of both. It is possible to characterize the microstructures in relation to the powder particle size. The coarser powders ($+40\,\mu$m) were generally cellular with a fine intercellular spacing (typically $< 1\,\mu$m) but also present were elongated regions of segregation-free solid, see Fig. 2a. Similar structures were observed as the particle size decreased, although not all powders contained segregation-free regions (Fig. 2b, for example). In the finer powders a higher proportion of segregation-free solid was apparent but unlike the coarser powders, growth of the solidification front appeared to have occurred behind a convex or near hemispherical plane front. The example in Fig. 2c shows a section of powder with dual morphology, the foil plane is approximately 90° to the growth direction during solidification and hence shows a circular featureless area. It was only in the finest powder ($< 3\,\mu$m cross-section) that completely segregation-free particles were observed.

Theoretical research (e.g. [6, 7]) in recent years has brought about a better understanding of the thermal history during solidification of atomized liquid metal droplets. Moreover, it has become apparent that large nucleation undercoolings can be achieved irrespective of external heat extraction rates [8]. Therefore, solidification of the majority of atomized powders is governed by the degree of undercooling and recalescence, and microstructures are created that strongly reflect that influence. It has been suggested that only

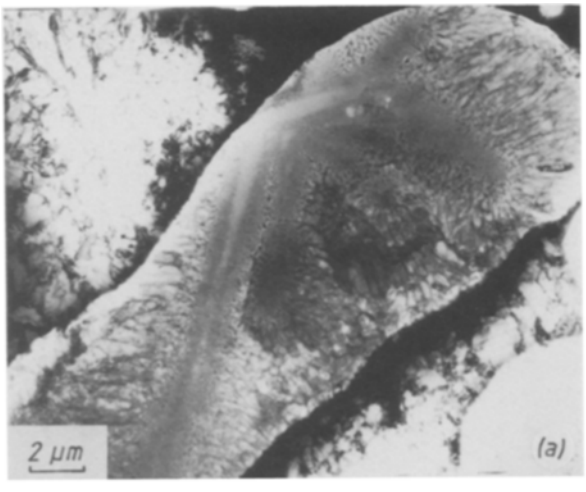

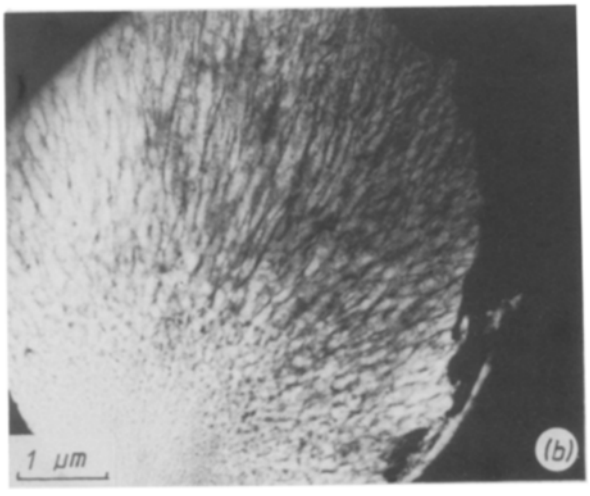

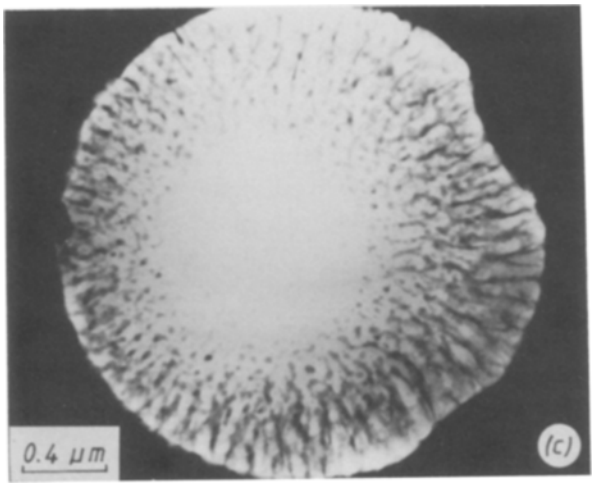

Figure 2 HVEM micrographs: (a) coarse powder ($+40\,\mu$m), (b) medium powder ($+12$ to $25\,\mu$m) and (c) fine powder ($-6\,\mu$m).

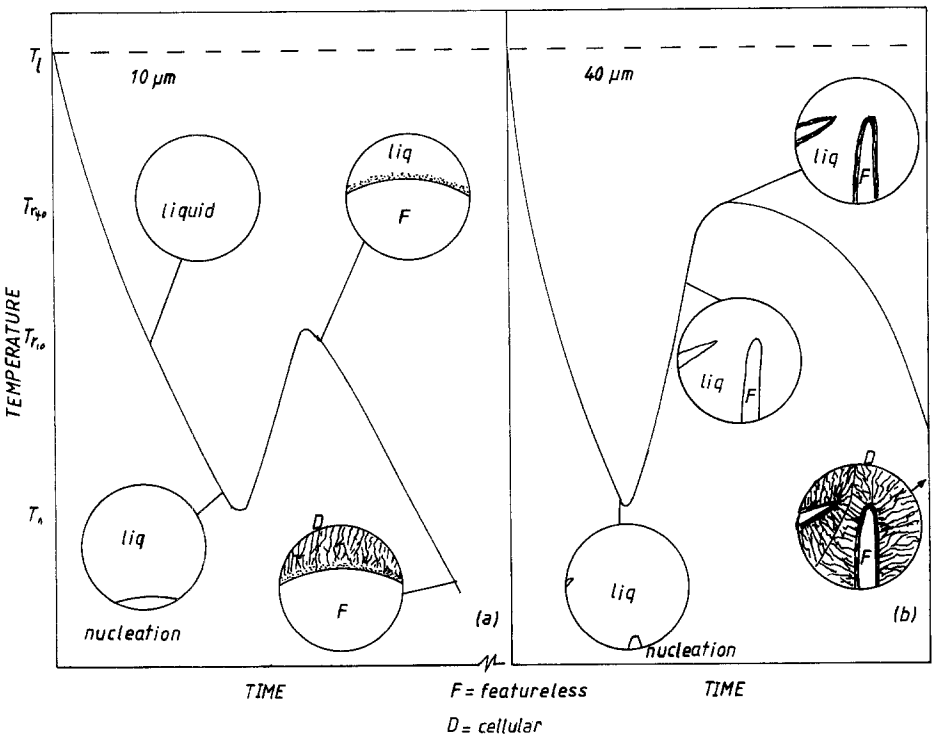

Figure 3 Schematic representation of solidification behaviour: (a) 10 μm powder, (b) 40 μm powder, F = featureless, D = cellular.

in the finest powder of a typical atomized batch can solidification of hypercooled droplets prevent recalescence and this has been confirmed by recent experimental observations [5, 9].

The solidification behaviour of the Al–Fe–Cr–Zr powder can be interpreted by examining two powder sizes, 10 and 40 μm. It is anticipated that the 10 μm powder will achieve a large undercooling prior to solidification, Fig. 3a, such that a strong driving force for growth exists once nucleation occurs. The driving force produces a high solid/liquid interface velocity which causes partitionless solidification and hence segregation-free solid. During initial solidification the droplet recalesces (Fig. 3a) and eventually the solidification is no longer partitionless. As the maximum recalescence temperature (t_{r10}) is reached a fine, segregated structure forms ahead of the partitionless–planar interface. Subsequently, the remaining liquid solidifies during the post-recalescence period behind a cellular interface at a growth rate determined by heat extraction to the cooling gas. The resultant microstructure contains a dual morphology, featureless and cellular, as shown schematically in Fig. 3a.

Observations from a number of powder particles indicated that nucleation occurred at the particle surface in the majority of cases. Clearly the atomization process had been effective in distributing potential nucleants such that nucleation occurred either homogeneously within the droplet or heterogeneously at the droplet surface. In general, the large droplet sizes have a greater probability of being influenced by nucleants and the achievable undercoolings would thus be affected. However, it has been reported [10] that reasonable undercoolings have been obtained in relatively pure aluminium droplets of 100 μm and clearly it is possible that a proportion of the large droplets will achieve undercoolings in the present alloy. Indeed microstructure in the Al–Fe–Cr–Zr coarse powder showed that nucleation still occurred heterogeneously at the surface of many droplets, see Fig. 2a, indicating that nucleants had been avoided and thus suggested that some degree of undercooling had been achieved. Typical of coarse powder was the initial formation of segregation-free solid at the droplet surface and then plane front growth away from the edge. Multiple nucleation events were commonly observed in the coarse powder which agrees with Levi and Mehrabien's conclusion [6] that larger particles are more likely to develop polycrystalline structures. Multiple nucleation and the needle-like morphology of the segregation-free regions can be explained in terms of the coarser powders' thermal history, shown schematically in Fig. 3b. Upon nucleation in the undercooled droplet, recalescence affects a local region around the solid–liquid interface and although a temperature rise occurs, it is initially localized leaving the bulk of the particle undercooled. A recent numerical analysis [6] has shown that temperature gradients are theoretically possible and during initial solidification the bulk of the droplet remains at the undercooled temperature. Furthermore, other nucleation events and growth of solid into the undercooled liquid will be encouraged. Hence, a high growth rate can be maintained and segregation-free solid created. However, as the average temperature of the droplet increases, the interface velocity is reduced until the plane front yields to microsegregation. At the maximum recalescence temperature (T_{r40}) the structure consists of featureless matrix enveloped in a thin film of the fine segregated structure. A cellular solidification front is created and the remaining liquid solidifies at 90° to the original growth direction. The final structure is again governed by the rate of heat loss to the cooling gas. Obviously some of the coarse powders experienced insufficient undercooling and uniform cellular microstructures were created.

Finally, it is worthy of note that this is the first report, to the author's knowledge, of segregation-free

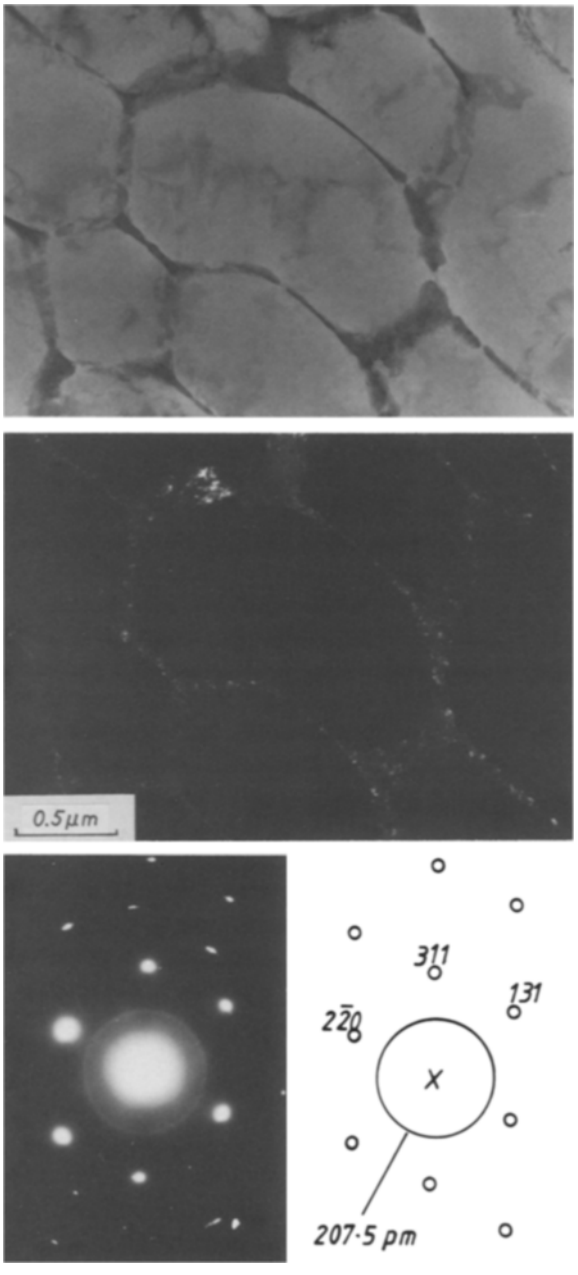

Figure 4 TEM showing cellular structure in a coarse powder with the appearance of precipitation at the cell boundaries (see text for details).

solid in relatively coarse (+40 μm) atomized powder. Hence it is apparent that the Al–Fe–Cr–Zr alloy is more susceptible to partitionless solidification.

3.2. Phase identification and elemental distribution

X-ray analysis indicated that no equilibrium phases were formed in the powder during rapid solidification. However, unassigned reflections were observed at *d*-spacings of 206 to 209 pm, 211 to 218 pm and 245 pm; only the latter was a well-defined peak. Although all three size fractions were separately assessed, no significant differences were discerned with the one exception that the unidentified, non-matrix peaks were less intense in the finest powder fraction. These additional reflections also corresponded to a ring diffraction pattern recorded during electron microscopy. The strongest diffracted ring (d = 207.5 pm) was used to obtain the dark-field image shown in Fig. 4 and quite clearly originates from the individual precipitates at the cell boundaries.

STEM microanalysis of cell structures, like the example in Fig. 4, provided the elemental distribution information given in Table I. The Scheil equation (or non-equilibrium lever rule) [11] was used to calculate the predicted data also given in Table I. The partitioning of iron and zirconium is in agreement with the predicted behaviour for eutectic and peritectic systems, respectively. In contrast, the behaviour of chromium deviates from the predictions with a high cell-boundary concentration but this may be artificially high because of contributions from the adjacent matrix. However, precipitation of $Al_{13}Cr_2$ in the intercellular regions during heat treatment (discussed later) does confirm some chromium enrichment.

The lattice parameter of the aluminium matrix also reflects the distribution of the three alloying additions, Table II. Both chromium and iron contract the aluminium matrix whilst zirconium causes an expansion, each element to a varying degree. Data showing the influence of each element are available [12] and can be converted for the alloy using the experimentally determined concentrations (Table I). The matrix concentrations for chromium, iron and zirconium yield changes of −1.24, −0.17 and +0.48 pm, respectively. Hence taking the cummulative effect gives a lattice parameter of 404.01 pm, using pure aluminium as 404.94 pm [12]. Whilst the simple assessment gives good correlation with experimental observations, it should be noted that different powder microstructures may exhibit varying solute levels, in particular the segregation-free solid.

The most significant result is the retention of chromium and zirconium in solid solution in a cellular structure, the most common observed in atomized powders. A previous study on the Al–Cr–Zr system [13] reported solubility extensions for substrate-quenched alloys but presumably in regions experiencing partitionless solidifications. Furthermore, Al–Cr–Zr alloys have been shown to age harden during solid state decomposition, whether as splat quenched or powder material [14], and the strengthening attributed to zirconium precipitation. Hence the Al–Fe–Cr–Zr

TABLE I Solute distribution in cell microstructure (wt %)

	Fe		Cr		Zr	
	Calc.*	Expt.	Calc.*	Expt.	Calc.*	Expt.
Matrix (centre)	0.07	0.38	6.34	3.02	2.60	2.31
Cell boundary	5.00	9.28	0.01	4.12	0.28	0.23
Alloy composition	–	2.59	–	3.30	–	1.30

* $C_s = C_0\, k\, (1 - f_s)^{(k-1)}$, k values from Mondolfo [12].

TABLE II (a) Variation in matrix lattice parameter with annealing

	As-Received	24 h, 350° C	1 h, 450° C	1 h, 550° C
a_0 (pm)	404.0	403.9	404.6	405.1

TABLE II (b) Phase transformations during annealing

Phase	As-Received	24 h, 350° C	1 h, 450° C	1 h, 550° C
Unidentified	medium	medium	n d	n d
$Al_{13}Cr_2$ (ASTM 29-14)	n d	weak	medium	strong
$Al_{13}Fe_4$ (ASTM 29-42)	n d	n d	weak	medium
Al_3Zr metastable	n d	medium	*	*
Al_3Zr (ASTM 2-1093)	n d	n d	n d	medium

* Reflections masked by aluminium matrix, presence confirmed by electron diffraction at 450° C.

alloy should offer the potential for precipitation hardening.

3.3. Structural changes during heat treatment

Samples of the powder were annealed at 350, 450 and 550° C for 1 h duration. However, no significant change occurred at 350° C and a further heat treatment of 24 h was performed, because age hardening had been reported previously [14] for this treatment.

The phases detected and the changes in matrix lattice parameter are given in Table II. The reflections from the unidentified phase(s) were unchanged after heat treatment at 350° C but were then replaced by reflections from $Al_{13}Cr_2$ and $Al_{13}Fe_4$ at 450 and 550° C. The zirconium precipitated as metastable Al_3Zr at 350 and 450° C, whereas the equilibrium phase was formed at 550° C. The increased lattice parameter with increasing temperature reflects the removal of solute (chromium and iron) and growth of second-phase particles.

Fig. 5 shows typical microstructures from powder annealed for 24 h at 350° C. The most significant feature was the precipitation of Al_3Zr in regions that were originally segregation-free, both in fine (Fig. 5a) and coarse powders (Fig. 5b). The fine scale of the precipitates (< 100 nm) is ideal for strengthening provided that it can be produced in a consolidated product. Transformation had occurred in some cellular regions, see Fig. 5a, and the X-ray results suggest this is $Al_{13}Cr_2$. The dual morphology was maintained at 450° C and again fine precipitates of Al_3Zr were formed whilst significant precipitation occurred in the initially cellular structure, Fig. 6a. The electron diffraction pattern, Fig. 6b, confirmed the formation of the metastable Al_3Zr phase which has a cubic $L1_2$ crystal structure ($a = 405$ pm). Electron diffraction from the coarser precipitates originating from the cell boundaries confirmed the presence of $Al_{13}Cr_2$ as both plate and spherical particles. After heating at 550° C the microstructure was more uniform and generally exhibited coarse plates of the intermetallic phases, see Fig. 7. However, the originally segregation-free solid (arrowed on Fig. 7) contained much finer precipitates because of the lack of heterogeneous nucleation sites which delayed precipitation. Similar morphologies were also observed in the finer powder where precipitates were apparently formed by homogeneous nucleation in the segregation-free regions.

In situ heating of the powder in a compacted state gave further details of the structural changes and in particular highlighted different transformation rates for contrasting starting microstructures. An area of relatively coarse cellular microstructure is shown in Fig. 8 during heating at 400° C. Rapid heating (5 min) to 400° C prevented transformation, see Fig. 8a, but after 15 min at temperature the first changes were noted. The initial structural change is the growth of discrete precipitates in the cell boundaries. After 30 min fine precipitation was seen within the cells, Fig. 8b, which clearly had nucleated homogeneously.

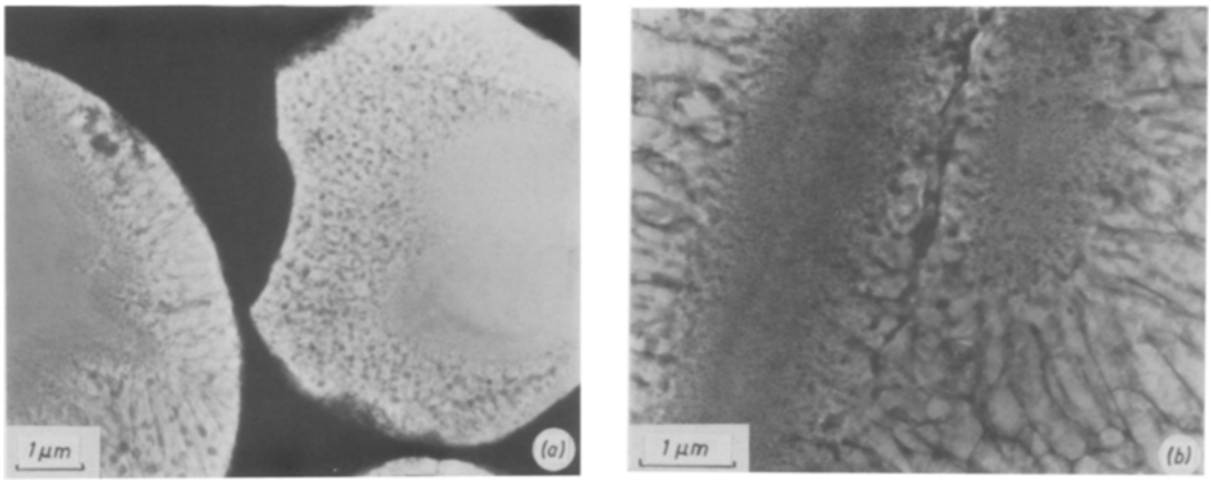

Figure 5 Powder annealed for 24 h at 350° C: (a) fine, and (b) coarse powder.

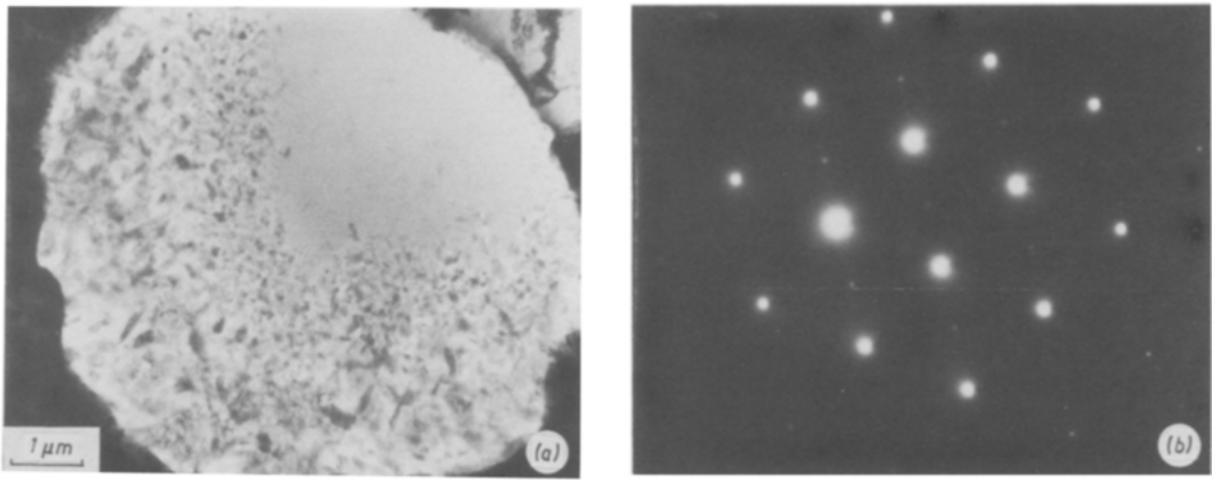

Figure 6 Powder annealed for 1 h at 450° C: (a) transformed solidification structure, and (b) [0 1 1] diffraction pattern showing superlattice reflections from the Al_3Zr phase.

During further heating the cell structure completely transformed to a distribution of relatively coarse plate and needle-shaped particles and a finer matrix precipitation of similar morphology, Fig. 8c.

Fig. 9 shows the behaviour during heating at 450° C of a small powder particle which exhibited a dual morphology, cellular and segregation-free. After 30 min both regions had transformed, Fig. 9a, with coarse precipitates created from the elongated cells and a high volume fraction of fine precipitates formed in the initially segregation-free solid. Further heating created little change in the coarser region but in the fine precipitate region a number of coarser precipitates had grown, Fig. 9b. It was only after 90 min that the microstructure had become more uniform within this particular powder, see Fig. 9c. However, between the coarse particles in the originally segregation-free region fine precipitation remained which was not observed in the structure developed from the cellular area.

The observations during heat treatment indicate two important features; very fine precipitation was generally confined to regions originally segregation-free and cellular starting structures transformed to a distribution of relatively coarse precipitates. In the cellular structure preferential nucleation and/or growth occurred at solute-rich boundaries and it was only in the larger cells of the coarse powder that homogeneous nucleation occurred, presumably because these regions were rich in zirconium. In the areas of segregation-free solid, predominantly homogeneous nucleation resulted with the consequent fine precipitation. During annealing some precipitates preferentially coarsen, those bearing chromium and iron, while the fine precipitates of Al_3Zr remained stable for the conditions examined. This is shown in Fig. 10 where fine precipitation of Al_3Zr was present between the coarser particles after annealing at 450° C. Hence it would appear that despite the retention of chromium and zirconium in solid solution during cellular solidification (see Table I) few benefits will be gained unless the mode of precipitation can be controlled. If predominantly homogeneous nucleation can be encouraged, then a fine stable dispersion of the metastable Al_3Zr phase can be created.

Clearly the transformations observed may be modified when the effects of heating and mechanical deformation are combined during consolidation. Research aimed at studying the consolidation behaviour and mechanical properties of this alloy is currently in progress.

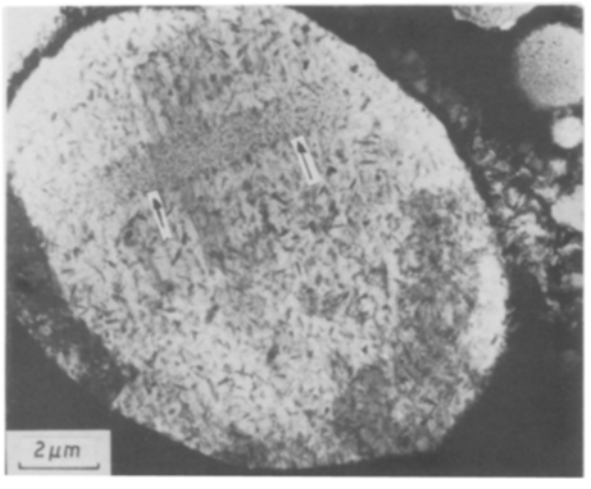

Figure 7 Coarse powder structure after 1 h at 550° C.

4. Conclusions

1. The powders exhibited two forms of solidification microstructure, cellular or featureless, and most particles contained a mixture of both.

2. The solidification behaviour has been interpreted as a function of powder particle size. In finer powders a large nucleation undercooling produces partitionless solidification at a high-velocity front but breakdown during recalescence creates cellular solidification and a resultant dual morphology within individual powders. In larger powders partitionless solidification was also observed, the first such observation in relatively coarse atomized aluminium powders, but an elongated morphology was formed due to localized recalescence which created a temperature gradient into the droplet and preferential growth.

3. An unidentified phase (or possible phases) was discovered in the atomized powder at cell boundaries which quantitative analysis showed to be iron and

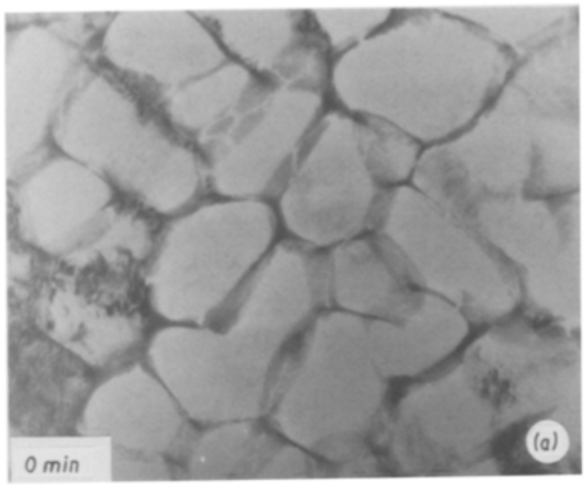

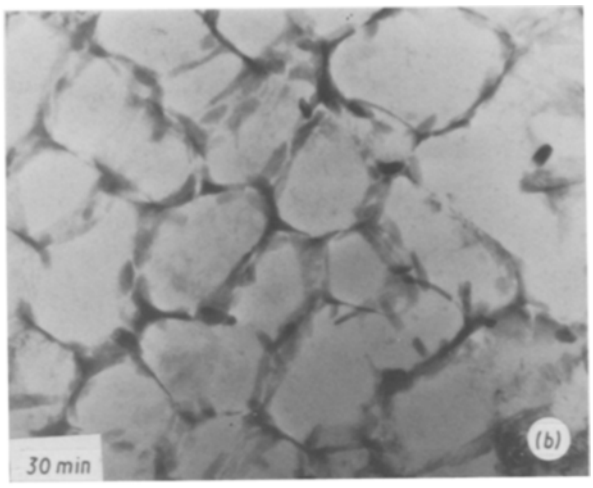

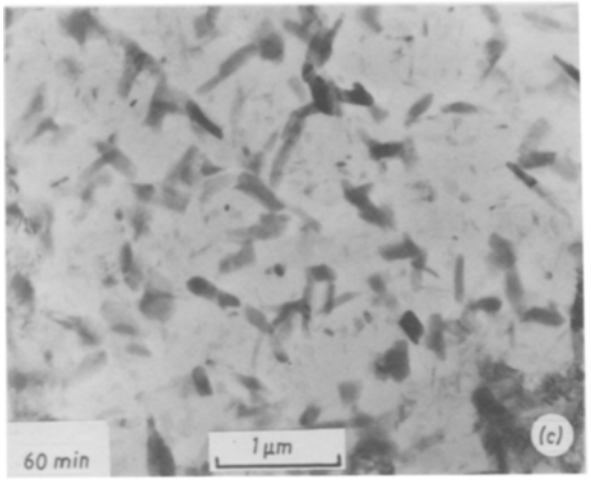

Figure 8 Transformation behaviour of cellular structure during *in situ* heating at 400° C.

chromium rich. Zirconium and some chromium were retained in solid solution within the cell matrix.

4. During heat treatment at 350° C a metastable Al_3Zr phase precipitated, while at higher temperatures the equilibrium $Al_{13}Cr_2$ and $Al_{13}Fe_4$ phases replaced the reflections from the unidentified phase(s).

5. Microstructurally, the initially segregation-free solid developed a mixture of fine Al_3Zr precipitates and coarser $Al_{13}Cr_2$ and $Al_{13}Fe_4$ particles. In contrast, no fine precipitation was maintained in the cellular regions after extended heating because of preferential growth of coarse precipitation formed at cell boundaries.

Acknowledgements

The provision of research facilities by Professors Pashley and Sheppard is gratefully acknowledged. The research was financially supported by a Department of Trade and Industry contract.

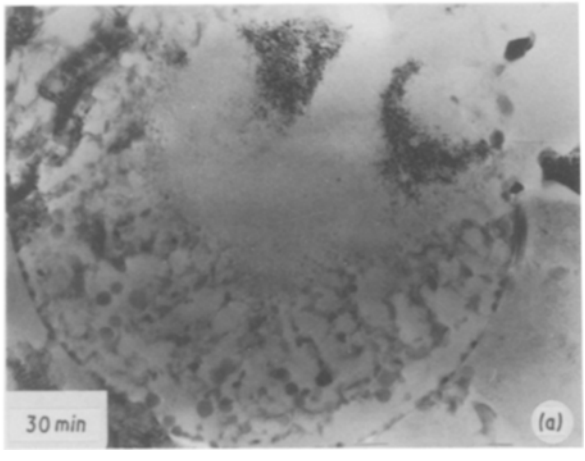

Figure 9 Transformation of fine powder structure during *in situ* heating at 450° C.

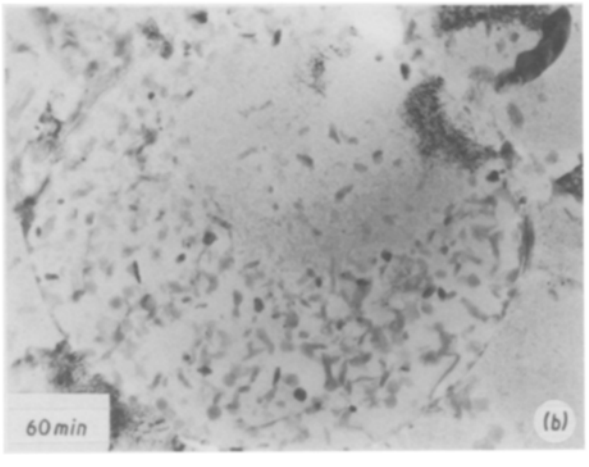

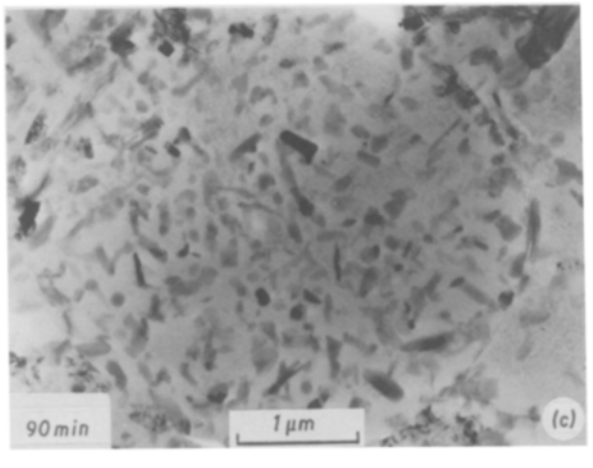

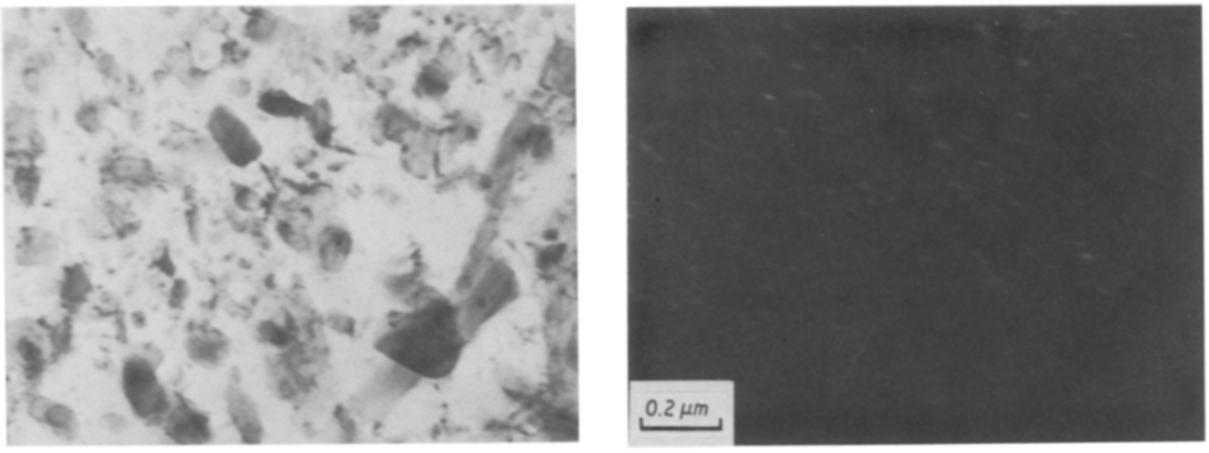

Figure 10 Precipitation of fine Al_3Zr particles in a coarser structure after annealing at 450° C.

References

1. C. M. ADAM in "Rapidly solidified amorphous and crystalline alloys", edited by B. H. Kear, B. C. Giessen and M. Cohen (Elsevier, Amsterdam, 1982) p. 411.
2. W. J. BOETTINGER, L. BENDERSKY and J. G. EARLY, *Met. Trans.* **17A** (1986) 781.
3. I. R. HUGHES, G. J. MARSHALL and W. S. MILLER, in "Rapidly Quenched Metals V", edited by S. Steeb and H. Warlimont (North-Holland, Amsterdam, 1985) p. 1743.
4. W. S. MILLER, European Patent 01 105 595, Alcan International, UK (1984).
5. G. J. MARSHALL, in "Aluminium Technology '86", edited by T. Sheppard (Institute of Metals, London, 1986) p. 679.
6. C. G. LEVI and R. MEHRABIEN, *Met. Trans.* **13A** (1982) 221.
7. T. W. CLYNE, R. A. RICKS and P. J. GOODHEW, *Int. J. Rapid. Solid.* **1** (1984-85) 59.
8. J. H. PEREPEZKO, S. E. LEBEAU, B. A. MUELLER and G. J. HILDEMAN, in "Rapidly Solidified Powder Aluminium Alloys", edited by M. E. Fine and E. R. Starke, ASTM-STP 890 (ASTM, Philadelphia, 1986) p. 118.
9. R. A. RICKS, P. M. BUDD, P. J. GOODHEW, V. L. KOEHLER and T. W. CLYNE, in "Al–Li III", edited by C. Baker, P. J. Gregson, S. J. Harris and C. J. Peel (Institute of Metals, London, 1985) p. 97.
10. J. H. PEREPEZKO, *Mater. Sci. Engng* **65** (1984) 125.
11. M. C. FLEMINGS, in "Solidification Processing" (McGraw-Hill, New York, 1974) p. 142.
12. L. E. MONDOLFO, in "Aluminium Alloys: Structure and Properties" (Butterworths, London, 1976) pp. 5–6.
13. S. P. MIDSON, R. A. BUCKLEY and H. JONES, in "Rapidly Quenched Metals V", edited by S. Steeb and H. Warlimont (North-Holland, Amsterdam, 1985) p. 923.
14. G. J. MARSHALL, I. R. HUGHES and W. S. MILLER, *Mater. Sci. Technol.* **2** (1986) 394.

Received 20 October 1986
and accepted 22 January 1987